



Effects of Holding Time on the Sintering of Cemented Tungsten Carbide Powder and Bonding with High-Strength Steel Wire

Mahadi Hasan , Jingwei Zhao, Zhenyi Huang, Hui Wu, Fanghui Jia, and Zhengyi Jiang

(Submitted January 10, 2019; in revised form April 28, 2019; published online June 26, 2019)

Cemented tungsten carbide (WC-10Co) and high-strength (AISI 4340) steel were successfully bonded by hot compaction diffusion bonding at a low temperature. The effects of holding time (5–50 min) on microstructure and mechanical properties of the sintered carbides and bonding strengths of the dissimilar bilayered composite materials were examined. The results show that the mechanical properties of the carbides increase, but the bonding strength increases firstly and then decreases with the increase in holding time. The maximum density and hardness achieved are 95.92 and 99.5%, respectively. A transitional layer forms at the interface as a result of elemental interdiffusion. The depth of the layer increases with the increase in holding time. The optimal bonding time is determined to be 40 min at a temperature of 1200°C and a pressure 160 MPa, by which the maximum bonding strength of 204 MPa of the WC-10Co/4340 steel joints can be achieved.

Keywords bonding interface, bilayered composite, elemental diffusion, microstructural characterization, powder–solid diffusion bonding

1. Introduction

Dissimilar bilayered composite materials can offer the combined advantages of two materials which are not attainable by a solitary material. A bilayered composite of cemented tungsten carbide (cermet) and steel can combine the properties of ceramics (e.g., hardness and wear resistance) and steel (e.g., toughness and strength). Such materials can be used as a structural component in the industry and domestic sectors, where both impact and wear resistance are required (Ref 1, 2). In tooling industry, for instance, where a bulk material (e.g., drilling or cutting tool) is used to provide mechanical support, a coating of hard material is used to prevent the wear resistance (Ref 3–6).

Cermets are conventionally joined with steel by solid-state joining techniques, usually by employing an interlayer. A number of different interfacial materials are reported to use which include Cu/Ag-based solders (Ref 7), multilayer brazing of Cu and Ni alloys (Ref 8–10), interlayer coatings of CrN, ZrN and TiC_xN_{1-x} (Ref 11), Ti interlayer (Ref 12) and electroplated Cu/Ni interlayer

(Ref 13). The chief reason of using such interlayer is to mitigate the mismatch of coefficient of thermal expansion (CTE) of these two materials. Due to large difference of their CTE values [$\sim 5.0 \times 10^{-6} \text{C}^{-1}$ for WC-Co (Ref 7) and $\sim 12 \times 10^{-6} \text{C}^{-1}$ for steel (Ref 14)], thermally induced residual stresses entrap at the joining interface during solidification process. This causes creation of micro-cracks and delamination at the bonding interface, leading to reducing the bonding strength and ultimately failure of the composite (Ref 8, 15, 16). Some advanced techniques, reported to join ceramic and steel, include spark plasma sintering (Ref 17), plasma spraying (Ref 18) and pulse plasma sintering (Ref 19). These methods are based on solid-state bonding, involving intermediate fabrication steps, assembling and machining processes (Ref 20). Solid-state joining usually deals with easy geometrically shaped parts with limited usage in the view point of industrial applications. Applying an interlayer adds up further complexity and cost. Furthermore, solid-state joining requires to heat up the sample at a high temperature close to their melting points. In contrast, making use of powder metallurgy (PM) techniques can substantially reduce the temperature requirements (Ref 21). PM also offers the advantage of decreasing production cycle, producing near net shape parts, eliminating the need of an interlayer and thus saving the cost and production time. In addition, compared to the solid state, PM promotes higher interdiffusion of alloying elements between joining materials, leading to a stronger bonding.

Zafar et al. (Ref 22) examined the joining of WC-12Co with AISI 304 stainless steel, using a so-called microwave hybrid heating technique. Feng et al. (Ref 7) examined the diffusion bonding of WC-Co/Ni and stainless steel and achieved a maximum tensile strength of 195 MPa at 950°C for 80 min. Thomazic et al. (Ref 2) fabricated cemented carbides/steel composite materials by PM and investigated the effects of various parameters including composition, compaction pressure, heating rate, sintering temperature and duration. Similar research was also conducted by Pascal et al. (Ref 23). These investigations give guidelines on the effects of various experimental parameters, microstructure analysis and bonding mechanics. However, studies on bonding between

Mahadi Hasan, School of Mechanical, Materials, Mechatronic and Biomedical Engineering, University of Wollongong, Wollongong, NSW 2522, Australia; and School of Materials Science and Engineering, Anhui University of Technology, Maanshan 243002, China; **Jingwei Zhao**, **Hui Wu**, **Fanghui Jia**, and **Zhengyi Jiang**, School of Mechanical, Materials, Mechatronic and Biomedical Engineering, University of Wollongong, Wollongong, NSW 2522, Australia; **Zhenyi Huang**, School of Materials Science and Engineering, Anhui University of Technology, Maanshan 243002, China. Contact e-mails: mh001@uowmail.edu.au; jzhao@uow.edu.au; jjiang@uow.edu.au.

ceramic and steel material are still a scanty. The interfacial stability, microstructural characteristics, formation of phases and mechanical properties of such bilayered composites are still a scope of investigation, as available information is still inadequate. Moreover, to the best of our knowledge, there is no literature that explains the effect of holding time on bonding characteristics between cemented tungsten carbide and steel.

In this paper, WC-10Co and AISI 4340 steel bilayered composite was fabricated by a novel technique called hot compaction diffusion bonding (HCDB). The theory and working principle of HCDB is reported in Ref 1. The ceramics were used as powder and steel as solid. Since W molecules are bigger and heavier, using them in powder form has the advantages of sintering them at lower temperature and promoting elemental diffusion for bonding with steel (Ref 24). Fe, on the other hand, can easily diffuse into WC matrix at this temperature. Usually, complete densification of carbide powders is performed above 1300°C; a detail summary of synthesis and sintering of cemented tungsten carbide can be found in Ref 21. In the present study, we have used a low-temperature electrical sintering process where a combined effect of heating and pressurizing is implemented under a vacuum environment to speed up the consolidation process. The limiting temperature 1200°C was selected based on literature surveys and experimental results. As reported in Ref 25, tungsten carbide powders with an average particle size (APS) of 100 nm could be completely densified at 1200°C under 100 MPa pressure. This gives the evidence of the possibility of obtaining full densification at this temperature, with additional advantage of using binder materials. In addition, during experiment it was found that over 1200°C the machine exhibited malfunction when holding time reached over 20 min due to overheating. Thus, the limiting temperature was chosen to be 1200°C. Consequently, the limiting pressure was chosen to be 160 MPa, because the punches do not survive at higher pressure for longer holding times. Nonetheless, this pressure is considered to be sufficient comparing to previous reports to obtain full densification (Ref 25). Thus, while keeping the sintering temperature and compaction pressure at 1200°C and 160 MPa, respectively, effects of holding time (5-50 min) on microstructure and mechanical properties of both the sintered carbide and bonded joints are investigated. The interfacial interaction of alloying elements with each other at cermet/steel joints is characterized. It is hoped that the investigation can provide the reference for the joining of ceramic and steel dissimilar materials, and the manufacture of bilayered composite with better quality.

2. Experimental

Nanocrystalline cemented tungsten carbide powder and high-strength steel (HSS) solid wire were chosen as experimental materials. In WC-Co matrix, Co is added as a binder

material. It plays a significant role in not only determining the mechanical properties of the bulk but also contributing the solidification process. An increase in Co content reduces the hardness and increases the transverse rupture strength. Therefore, a proper balance of Co content is necessary. In most industrial applications, particularly in tool industries, Co is used in the range of 10-15%; presenting a decent compromise between the hardness and transverse rupture strength (Ref 26). In this study, we used WC-10Co powder of an APS of 100 nm, and AISI 4340 steel wire of 1 mm in diameter. The chemical compositions of these materials are presented in Table 1.

Figure 1 presents the schematic diagram of the experimental set up used in this study. In this process, a simultaneous effect of pressure and temperature is applied. The heating is generated using the Joule effect by passing an electrical current through electrically conductive samples. A continuously progressing pressure from both ends is applied to accelerate the solidification process at lower temperature and promote the bonding process. The sample is insulated by quartz tube as shown in

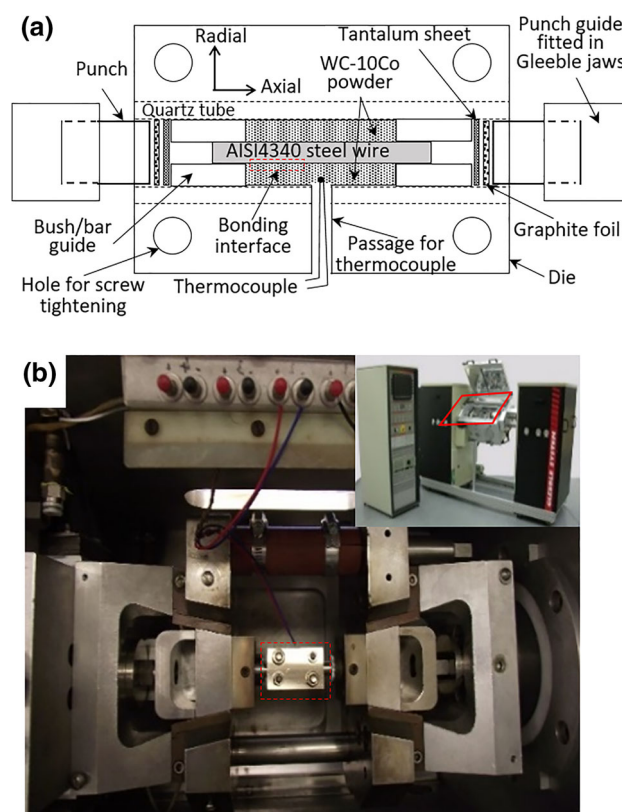


Fig. 1 Experimental setup: (a) schematic diagram of the HCDB process, showing various components of the die assembly and sample preparation mechanism, and (b) the experimental die setup is clamped by the two jaws of Gleeble 3500 thermal-mechanical simulator

Table 1 Chemical compositions of WC-10Co and AISI 4340 steel (wt.%)

Material	Fe	Co	C	Cr	Mn	Ni	N	Zn	Al	V	O	Mo	Si
WC	–	10.0	–	< 0.01	–	0.02	0.06	< 0.06	0.03	0.04	< 0.5	–	–
AISI 4340	Balance	–	< 0.4	< 0.8	0.7	< 1.8	< 0.1	–	–	–	–	0.25	0.25

Fig. 1(a) for limiting the heat conduction through the die set up. Thermocouples are used for controlling the temperature and machine functionalities as shown in Fig. 1(a). Gleeble 3500 thermal–mechanical simulator (Fig. 1b) was employed to carry out the experiment in a vacuum environment.

The interfacial microstructure of cermet and steel was observed by optical microscopy (OM, Keyence VK-X200) and scanning electron microscopy (SEM, JSM-7001F) equipped with backscattered electron. The distribution of chemical elements at the bonding interface was examined through Aztec Oxford energy-dispersive spectroscopy (EDS) elemental line-scan analysis. The phases formed during sintering process were identified by x-ray diffraction (XRD) using monochromatic Cu, K α radiation in GBC MMA diffractometer, with an angular step size of 0.05°, and a speed of 2°/m, at 35 kV and 28.4 mA. Tracesv6 ver. 6.6.10 was subsequently used for phase analysis.

The mechanical properties were evaluated by examining the microhardness, density, porosity and bonding strength calculation of the bilayered composite. The microhardness indentations were carried out across the sample as shown in Fig. 2(a), using a Struers Durascan Vickers microhardness tester under a load of 4.9 N and dwell time of 10 s. The mechanical shear bonding strength was calculated by a set up as shown in Fig. 2(b). The setup is mounted on a high-precision micro-tensile machine, and Eq. 1 is used to calculate the bonding shear strength.

$$\sigma_{\text{bonding}} = \frac{F_{\text{maximum}}}{A_{\text{bonding}}} \quad (\text{Eq } 1)$$

where σ_{bonding} is the shear bonding strength in MPa, F_{maximum} is the maximum load recorded in micro-tensile testing machine in N, and A_{bonding} is the shear bonding results and discussion.

3. Results and Discussion

3.1 Thermodynamic Analysis

Selection of appropriate compositions and sintering conditions is imperative for obtaining desired mechanical properties and make a successful bonding between the ceramic and steel materials. The mechanical properties, such as hardness and toughness, and wear resistance of cemented carbides can be essentially improved, and the sintering temperature to attain full density can be considerably decreased, when the particle size of the initial carbide powder is smaller than sub-micron scale (Ref 27, 28). In fact, the use of superfine and/or nanoscale powders

with particle size smaller than 500 nm is getting a continuously growing interest in the field of metal machine, tool industry and medicine for their outstanding properties (Ref 29). As nanocrystalline cermet with 100 nm particles size may have even better performance, it has become a hot topic in the field of refractory and hard materials worldwide. The possibility of obtaining full density of such materials at a temperature as low as 1200°C is also addressed by a number of researchers (Ref 27, 30). Consequently, when considering the fact of bonding, both the nanocrystalline cermet and steel should be processed in similar sintering conditions. The temperature is required to be lower than the melting point of both materials, however, it has to be high enough to reach the full density of the cermet and adequately promote interdiffusion of alloying elements for bonding to occur with the steel (Ref 1). Based on the above analysis, we have chosen the temperature of 1200°C for sintering nanocrystalline (100 nm APS) cermet powder and bonding with AISI 4340 steel.

The second stage is to predict/simulate the characteristic phases and compositions that may form (particularly at the interface) under the selected temperature, leading to produce the microstructure, which in turn, directly affects the mechanical properties of the composite. Such simulation also helps to understand the microstructural behaviors of the composite in advance and compare with the experimental findings. Phase equilibria data are utilized to perform such analysis and determine the possible compositions and phases in a given temperature. Calculation of phase diagram (CALPHAD) method is one of the popular techniques for selecting models that can define the equilibrium state of the material system with thermodynamic functions that, by principle, rely on temperature, pressure and composition (Ref 31). Using the CALPHAD method, a consistent thermodynamic description of W-Fe-C and W-Co-C ternary systems is presented in this study. Figure 3 presents an isothermal section of the ternary phase diagram (TPD) of W-Co-C simulated at 1200°C, and a vertical section of TPD with 10 mass percent Co. The simulation was conducted by Thermo-Calc software, version-2018a using TCFE9 database. Compositions are given in atomic fractions, and the phases obtained by simulation are mentioned.

It is reported that the conditions close to equilibrium prevail at temperatures typically above 1000°C in cemented carbide sintering, owing to the short diffusion distances involved (Ref 32). According to W-Co-C ternary diagram (Fig. 3a), η phase (M_6C) can form at a lower carbon content at a given temperature of 1200°C. It is apparent that carbon content is important, changes of which result in different phases to form. By increasing the carbon content, a narrow two-phase region of

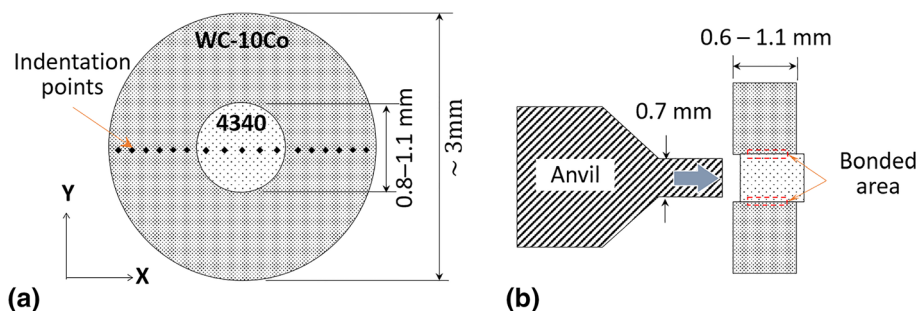


Fig. 2 Schematic diagram of mechanical properties evaluation, (a) cross-sectional view of the sample showing the microhardness indentation points, and (b) testing setup mounted on high-precision micro-tensile for determining shear bonding strength

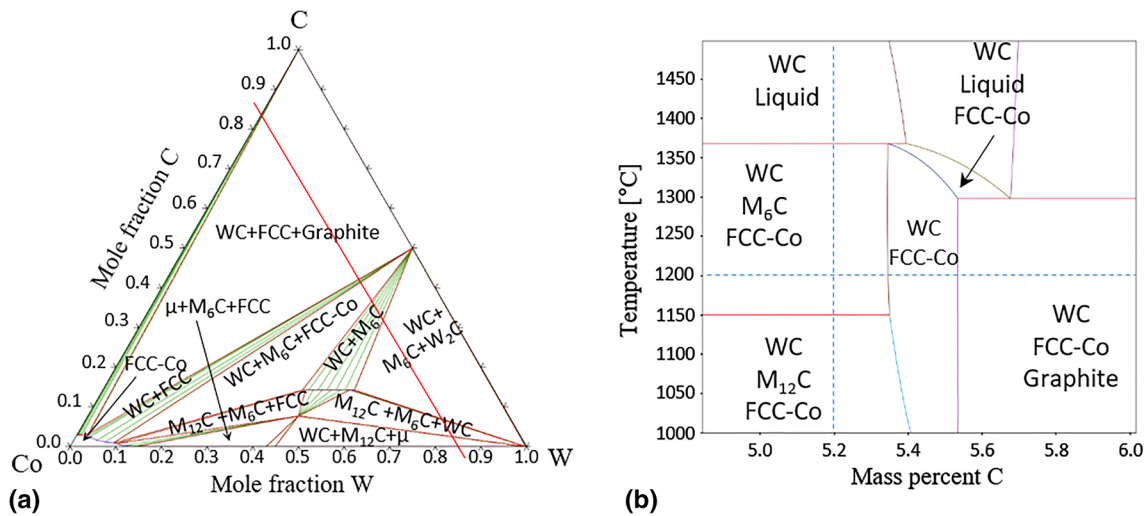


Fig. 3 Thermodynamic system of W-Co-C: (a) isothermal section of the ternary phase diagram W-Co-C at 1200°C, and (b) vertical section of the ternary phase diagram W-Co-C at 10 mass% Co, showing the possible phases that can form during sintering process

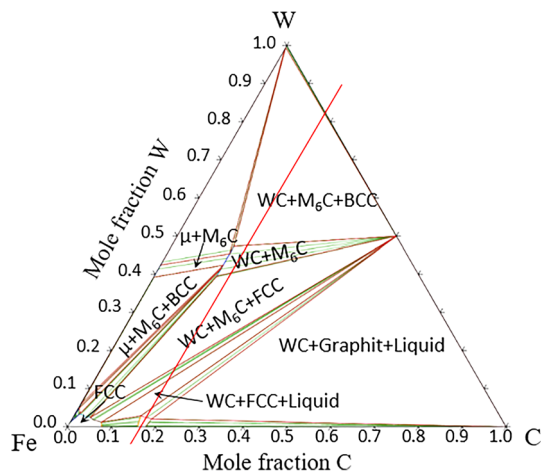


Fig. 4 Thermodynamic isothermal section of the ternary phase diagram of W-Fe-C system simulated at a temperature of 1200°C, showing the possible phases that can form during the sintering process (Color figure online)

binder and WC can be reached, without forming intermetallic η phases. Further increase in carbon content generates graphite formation. For cemented carbides with binder (Co) content, the effect of carbon content can be examined by sectioning the ternary diagram by assuming fixed Co content. The red line as shown in Fig. 3(a) presents 10 mass% Co, corresponding to 0.156 mol fraction. The binary phase diagram obtained from the vertical section of the ternary system provides the information of equilibria in the temperature range from solid to liquid state. Figure 3(b) shows stable phases presented as a function of temperature. The stoichiometric mixture corresponding to WC-10 mass% Co, is 5.52 mass% C (Ref 33). The η phase free, two-phase (WC + FCC-Co) region is limited to carbon content range of 5.4-5.57 mass%. It is usual that some carbon reacts with oxygen and reduces carbon percentage. However, conducting experiment in vacuum environment gives the advantage of not losing the carbon content (Ref 33).

Figure 4 presents the typical isothermal TPD sections of W-Fe-C system simulated at 1200°C. An indication of the phases

that can form at the interaction of cermet and steel is estimated. It is hard to know the exact percentage of the carbon taking part in the reaction at the interface; therefore, an equal proportion of WC and Fe are considered. This gives a stoichiometric percentage of carbon content of 0.18 mol fraction; the line is presented in Fig. 4 by red color. A three-phase region owing to liquid formation is observed which narrows down with the increase in W content. During bonding, the formation of liquid phase is beneficial to stimulate the adhesion and joining process (Ref 23). However, the liquid fraction must be limited in amount by controlling the holding time to retain the sample geometry. With lower carbon content, intermetallic phase (e.g., Fe_7W_6) and ternary η phase (e.g., $\text{Fe}_6\text{W}_6\text{C}$, $\text{Fe}_3\text{W}_3\text{C}$) are expected to form. As reported in Ref 14, these phases are stable down to room temperature and important for bonding of cermet and steel. The accuracy of the prediction is reflected in the results of phase identification of the fabricated composite and illustrated in subsequent sections.

3.2 Microstructure

Figure 5 presents a typical general view (OM) of the microstructure at the bonding interface sintered at 1200°C under a pressure of 160 MPa for 40 min. The left side presents cermet, and the right side is steel. As shown in Fig. 5(b), grains and grain boundaries of the steel part are clear after etching. Grain boundaries of WC-10Co are not visible in the OM micrograph due to their nanocrystalline sizes which are not covered by OM resolution. It is found that in all experimental conditions, bonding between cermet and steel takes place. However, their mechanical properties and bonding characteristics vary substantially with the increase in holding times. From the OM micrograph, it is clear that defects, such as cracks and stripping, are not observed along the bonding interface of WC-10Co and AISI 4340. It is apparent that the powder-solid diffusion bonding, using compaction diffusion bonding process, can lessen the effects of residual stresses caused by CTE discrepancy of cermet and steel and therefore result in a successful bonding between them. In addition, non-appearance of any visible discontinuity or defects at the interface also indicates a good interdiffusion during the sintering processes. Some microvoids, however, are still present

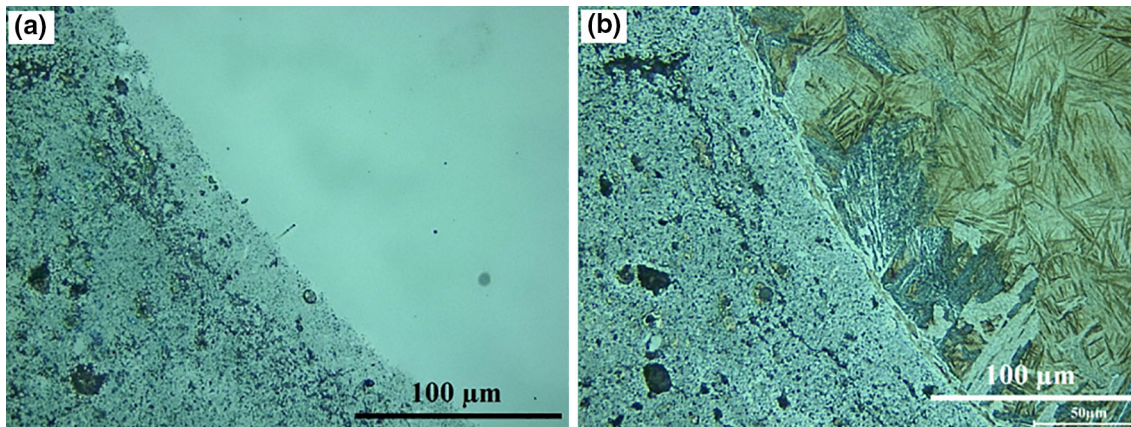


Fig. 5 Interfacial OM micrograph of polished and etched sample sintered for 40 min (a) polished to quarter micron, and (b) etched in Nital solution, showing the upper bainitic microstructure of AISI 4340

in the carbide region, indicating incomplete densification in those regions. From the microstructure of the etched steel (Fig. 5b), the formation of upper bainite is evident. A likely explanation is: carbon is rejected to austenite surrounding the bainitic ferrite laths since the solubility of carbon in bainitic ferrite is lesser than in austenite. When concentration of carbon in austenite increases, cementite starts to nucleate as discrete particles or discontinuous stringers at the ferrite/austenite boundaries. With further increase in C, the cementite filaments, surrounding the bainitic ferrite laths, become more and more numerous and continuous. The structure looks like a pearlite and is called as feathery or upper bainite (Ref 34). This observation is analogous to the CCT diagram of AISI 4340 steel (Ref 35), based on the cooling rate, the carbon content and the temperature applied in this experiment.

Figure 6 exhibits the microstructure and EDS linescan distribution of the elements across the bonding interface of WC-10Co/AISI 4340 bilayered composite. The images are taken with the same magnification, where light-gray contrast presents WC-10Co and deep-gray contrast is AISI 4340 steel. As can be seen from the SEM images, bonding between the cermet and steel, without any defect, is achieved under all sintering conditions. The sintering and bonding quality, however, improve substantially with the increase in the holding time. It is found that the joining interface is not a straight line, rather a wavy or dentate shape. This specifies the characteristics of liquid-state sintering at the interface as predicted in Sect. 3.1, promoting interdiffusion of the alloying elements. In the case of dissimilar materials bonding, this interdiffusion process plays a significant role as it helps to assuage the influence arose from the difference of their physical properties (e.g., CTE) and eventually result in stable and strong bonding (Ref 36). The interdiffusion of elements also causes new chemical reaction to take place, leading to form new phases and a diffusional transition layer to appear at the bonding interface (Ref 23). The depth of such layer mostly depends on the materials to be joined, their compositions, applied sintering pressure and temperature and most importantly holding time (Ref 37). The constituents and properties of the phases that form at the interface are also crucial. Forming intermetallic phases is helpful for good bonding; however, too much of their presence may lead to the interface too brittle which is detrimental for the bonding.

Figure 6(a), (b), (c), (d) and (e) shows the representative images to demonstrate the effect of holding time on sintering

and bonding of WC-10Co/AISI 4340 steel bilayered composite sintered for 10-50 min, respectively, with a gap of 10 min, under a constant pressure of 160 MPa at temperature of 1200°C. According to holding time applied and their corresponding microstructural observations, the bonding interface obtained can be roughly classified into three stages: (1) holding time ≤ 20 , (2) $20 < \text{holding time} \leq 40$ min and (3) holding time > 40 min. In stage (1), the carbide area is attributed to poor sintering, owing to the presence of large amount of porosity. The reason of forming such porosity is inadequate densification. The holding time applied in this stage is insufficient leading to incomplete coalescence of powder particles. However, no visual cracks or discontinuities are found at the bonding interface. Non-availability of any visible diffusion layer also indicates insignificant migration of alloying elements during holding time of 5, 10 and 20 min. This microstructural observations are in well accordance with the results obtained by elemental distribution profiles. In order to analyze quantitatively the elemental distributions across the bonding interface, EDS linescans were performed by Aztec Oxford EDS, mounted on JEOL SEM 7001F. The results are presented at right hand of the corresponding SEM images. As can be seen (Fig. 6a-c), no significant elemental diffusion is detected except a tiny amount of Fe and Co. However, no noticeable W diffusion is found. In stage (2), a significant improvement is observed in the quality of sintering and bonding. The densification of cermet powder progresses considerably by allowing more sintering time under similar temperature and pressure conditions. The porosity is greatly reduced. Figure 6(c) and (d) presents the interfacial microstructures sintered for 30 and 40 min, respectively. No visible cracks or discontinuities are observed at the interface. It is observed that the appearance of the grains in the cermet regions becomes clearer with the increase in the holding time, as reported in Ref 29. The corresponding EDS elemental distribution profiles are shown in the right hand of Fig. 6(c) and (d). An increase in holding time leads to intensify the elemental diffusion across the bonding interface (Ref 38). As a result, the migration of the elements such as Co, Fe and W upsurges considerably, as identified by EDS linescans. A thin transitional layer of elemental diffusion is also appeared. This indicates pronounced intermigration of alloying elements taking place at the joining interface. Forming such diffusion layer compensates the issue of CTE mismatch by reducing the residual stresses trapped at

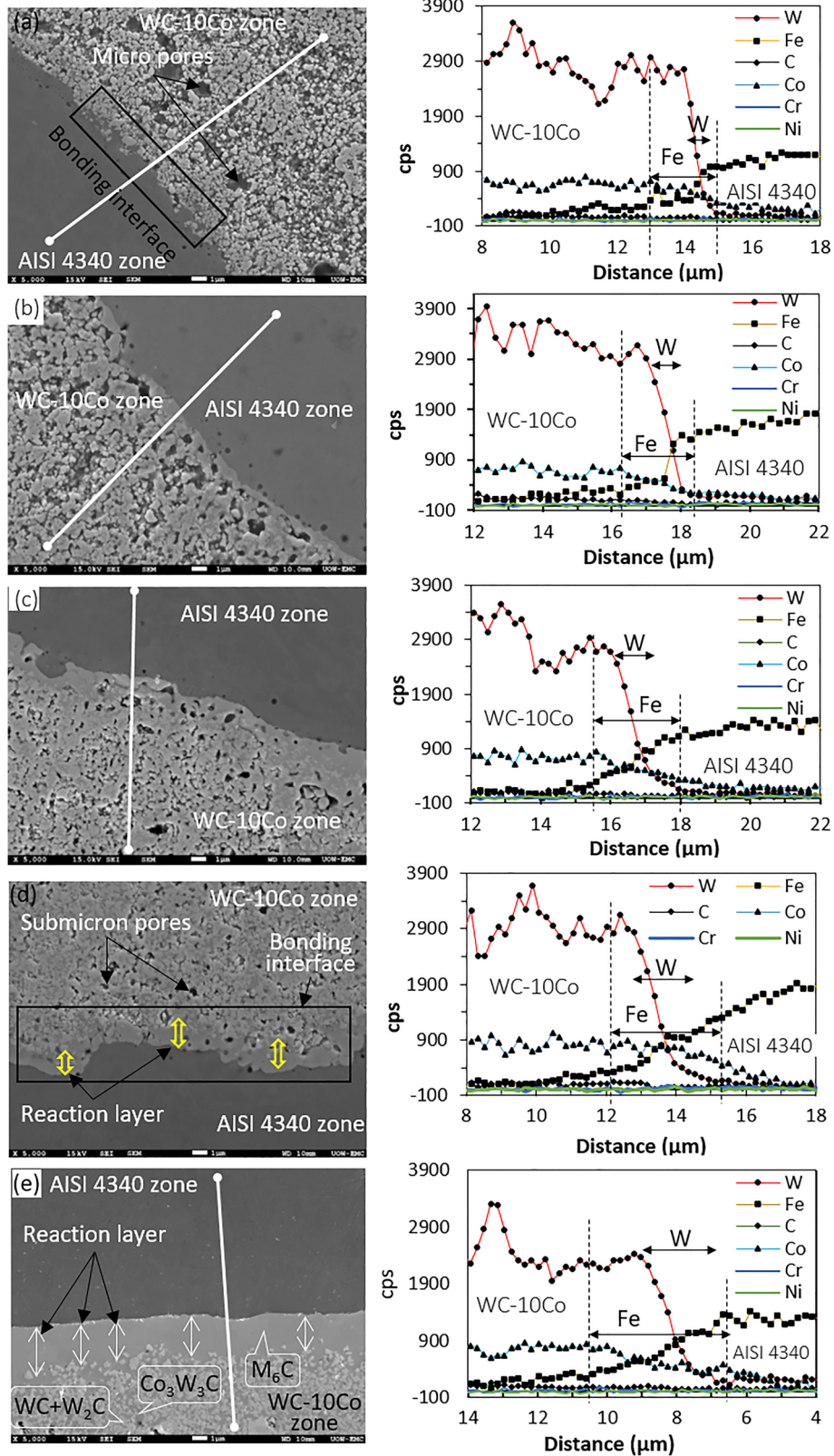


Fig. 6 SEM micrograph showing the microstructure at the bonding interface (left side) and their corresponding elemental line scan distribution (right side) of the samples sintered for (a) 10 min, (b) 20 min, (c) 30 min, (d) 40 min and (e) 50 min, at 1200°C under 160 MPa pressure

the bonding interface during cooling, which in turn, helps to achieve a stable and strong bonding between ceramic and steel materials. When sintering time reaches to 50 min (stage (2)), the consolidation process of powder particles is further improved. The porosities and voids are further reduced, contributing to near net shape sintered cermet. The microstructure is presented in Fig. 6(e). The diffusion of allowing elements is further intensified as identified by linescan results (right hand of Fig. 6e). This specifies that increment in holding time essentially enhances the diffusion process. The phenomenon is also reported in Ref 39 that the diffusion process during joining dissimilar materials is proportional to the sintering time. This is noteworthy that the waviness at the bonding interface is slightly reduced at holding time of 50 min. The possible explanation is the increase in transition layer, i.e., the waviness at the bonding interface is reduced with expense of forming diffusional layer at the bonding interface.

The diffusion mechanism is studied by elemental distribution across the interface. As can be seen (the right side of Fig. 6a-e), the EDS profile curves vary continuously and smoothly across the interface indicating the formation of solid solutions. The elemental diffusion area detected is marked with dotted lines. From the elements as mentioned in Table 1, only W, Fe and Co are found to participate actively in the diffusion process. The reason is their high volume presence in the mixture and concentration difference between the two regions. It is noteworthy that the diffusion depth of Fe into cermet region is higher than that of W into steel, in all cases. This is because of the difference of their molecular sizes. Takemoto (Ref 24) reported that the activation energy of the elemental diffusion is determined by their atomic sizes under similar sintering/experimental conditions. Similarly, Co elements penetrate in the direction to steel gradually. Though the diffusion of Co is observed in all conditions, however, enhances with the increase in holding time. These results prove mutual solubility of alloying elements, leading to cause intimate contact between ceramic and steel materials. Atoms from cemented carbide region to steel region and vice versa diffuse continuously toward each other across the interface during sintering process. When concentration of an element reaches a certain value, the element may in principle produce a new phase and form a transitional reaction layer in which the microstructure is different than that of the substrate regions (Ref 38). Consequently, a gradient microstructure is formed resulting in a stable bonding. The phases formed at the interface mainly consist of ternary intermetallic carbides which are identified and discussed in XRD phase analysis. One may also notice that the diffusion depth increases with the increase in sintering time from approximately 1 micron at holding time of 30 min to 3.5 micron at holding time of 50 min. According to diffusion kinetics and Fick's law, the diffusion coefficient of substrate elements and atoms vibrational energy enhances with the increase in holding time for a given temperature, which allows higher interdiffusion to occur at the interface (Ref 40). The line scanning results also demonstrate that the diffusions of the elements such as C, Cr and Ni are not obvious even at 50 min of holding time.

The typical full cross-sectional SEM images of the fabricated WC-10Co/AISI 4340 bilayered composite are presented in Fig. 7. Figure 7(a) and (b) presents the composite sintered with a holding time of 40 min and 20 min, respectively, at 1200°C, under a constant pressure of 160 MPa. EDS areal layered map, elemental mapsum and individual spectrums of

Fig. 7(a) are mentioned in Fig. 7(c), (d), (e) and (f), respectively. As can be seen from the full cross-sectional images, no visual crack or discontinuity observed at the interface regions. It appears that with the increase in sintering time, the quality of the composite improves substantially. In Fig. 7(b), sintered with a holding time of 20 min, a high volume of porosity and voids is present. In Fig. 7(a), sintered with a holding time of 40 min, the sample is fully densified with small amount of porosity. The agglomerated powders (white regions) are more dense and compact. EDS layer image presents the elemental distribution of W, Fe, Co, Cr, C and O elements. The spectrum shows the presence of W, C, Fe, Co, Cr, Ni, O and V, with the highest peak of W element.

Figure 8(a), (b), (c), (d), (e) and (f) presents the XRD results obtained at holding times of 5-50 min, respectively. The phases identified are mainly composed of eutectic carbides (WC and W₂C), Fe and so-called η carbides (M₆C, Fe₆W₆C, Co₆W₆C and Co₃W₃C). These phases are generally expected to form at the interface region of WC and steel at or above 1100°C, as reported in previous studies (Ref 41, 42). They possess bulk modulus such as 462 GPa for Co₆W₆C (Ref 43) which is higher than that for diamond (~ 444 GPa) and WC (~ 421 GPa) (Ref 41). The Vickers microhardness for Fe₃W₃C and Fe₆W₆C is found to be around 15.6 GPa (Ref 41). The formation of these phases and their amounts in the samples, therefore, have high technological importance in terms of mechanical properties and bonding stability (Ref 41, 44, 45). It appears that with lower holding time, such as 5 and 10 min (Fig. 8a, b), the phases are composed of only WC and cementite. Slow cooling (2°C/s) rate is thought to be the main reason for the formation of cementite from initial martensitic steel, as explained in Sect. 3.2. Increase in holding time causes new phases to form. When holding time is 20 min, η phases, including Fe₆W₆C, Co₆W₆C and Co₃W₃C form, and then M₆C (Fe₃W₃C) and W₂C form with a further increase in sintering time (Fig. 8c). Further increase in time does not generate any new phases; however, the presence of η phases is more pronounced as evident by higher diffraction intensities of the peaks (Fig. 8d-f). The reason of forming such M₆C (Fe₃W₃C) and W₂C during longer holding time can be attributed to possible decarburization of WC from initial powder owing to high temperature and pressure (Ref 22). This causes tungsten enrichment and local formation of M₆C at the bonding interface (Ref 23, 46). Here, it is noteworthy to mention that according to available crystallographic data (Ref 47-49), all the examined η carbides Fe₃W₃C, Fe₆W₆C, Co₃W₃C and Co₆W₆C adopt the cubic symmetry with the space group of Fd3 m (no. 227). The only difference between Fe₃W₃C, Co₃W₃C and Fe₆W₆C, Co₆W₆C is that they contain 16 and 8 carbon atoms (per cell), respectively (Ref 47-50). Comparing to the effects of holding times 40 and 50 min, the formation of M₆C expands considerably. These findings are also reflected in the results of microstructure analysis as shown in Fig. 6.

This is interesting to note that, though the nucleation and/or formation of all the phases is possible at 1200°C, as predicted by thermodynamic simulations (Sect. 3.1), however, they are not identified until the sintering time reaches to over 20 min. The likely explanation is that the intermetallic phases did not form due to nucleation and growth difficulties and/or were hindered by insufficient diffusion time for their growth at the temperature of interest, during hot compaction diffusion bonding process. Longer holding times may promote their formation (Ref 38). In addition, it is stimulating to note that the

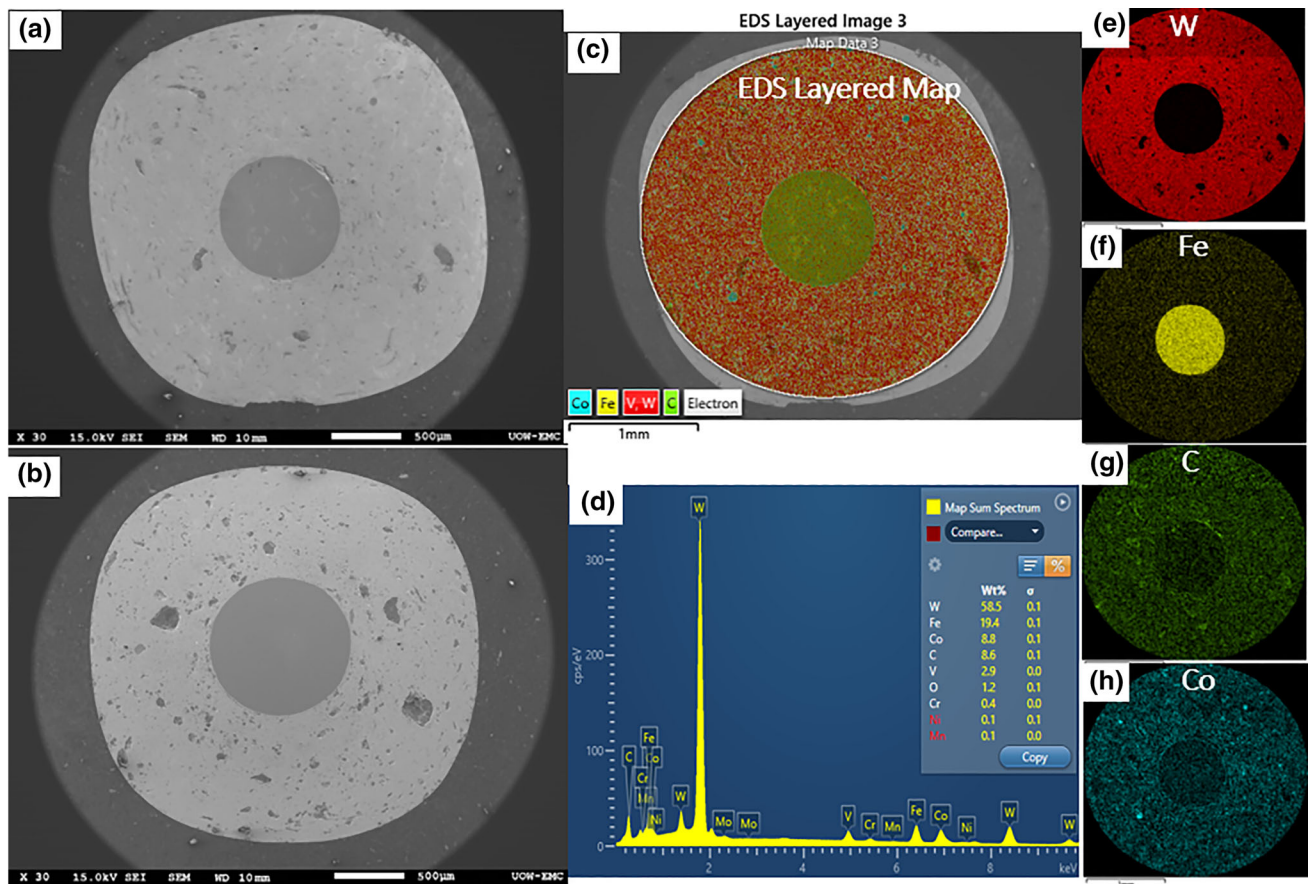


Fig. 7 Full cross-sectional SEM image of the bilayered composite of outer side WC-10Co and inner side AISI 4340 steel (a), (b) SEM image sintered for 40 min and 20, respectively, at 1200°C under compression pressure of 160 MPa, (c) EDS layered map of (a), (d) elemental map sum spectrum of Fig. 7(a), and (e)-(h) elemental spectrum of W, Fe, C and Co, respectively

diffraction intensities of the XRD patterns reduce gradually with the increase in holding times from approximately 610 to 190 for Fig. 8(a), (b), (c), (d) and (e). These indicate that the textures may have been changed with the increase in holding time, as reported in Ref 51. A small amount of peak shifting is also observed, indicating the presence of minor micro-strain in the fabricated bilayered composite, possibly due to applying a high and continuous compaction pressure. The crystallographic information and lattice parameters of the phases are obtained by Rietveld refinement using MAUD 2.79 software, and the results are summarized in Table 2. Since the samples are in solid form and miniature in size, the resolution of obtained XRD patterns is limited, resulting in a limited accuracy of the fitting. However, the residual being in the deviation range, with σ 1.3 and R_{wp} less than 20, the values should be considered as a good estimation.

3.3 Mechanical Properties

3.3.1 Bonding Strength. The bonding strength of the joints is determined by a tailor made apparatus mounted on micro-tensile machine at room temperature (Fig. 9a), and the results are presented in Fig. 9(b). Since the fabricated composites are miniature in size, cutting samples for direct tensile tests were not possible, instead a shear bonding strength test was conducted. For the specimen with holding time of 5 and 10 min, the tests were not completely successful, due to their

breakage at earlier stage of measurement. This is because of premature sintering of the carbide powders at these sintering times as discussed in Sect. 3.3.3. However, this is worth mentioning that the data presented in Fig. 9(b) for holding times of 5 and 10 min are the values that required to break the samples. Hence, they are mentioned to indicate the trend. The bonding strength measurements for the samples fabricated at holding time ≥ 20 min were successful and found to be continuously increasing with the increase in holding times until its maximum value reaches at 40 min. The average maximum bonding strength recorded is 203.81 MPa. The improvement can be attributed to increased contact between bonding surfaces. At 20 min of sintering time, the initial stage of interfacial diffusion occurred by forming a chemical bridge at cermet/steel surfaces. However, the contact between the surfaces was not enough for tight bonding due to insufficient sintering time. Allowing additional sintering time results in enhanced diffusion and more intimate contact. Consequently, the bonding strength of WC-10C/AISI 4340 steel composite increased. However, the bonding strength shows a downward trend beyond holding time of 40 min. When holding time reaches to 50 min, the bonding strength goes down, the bonding strength at this stage recorded is 195.29 MPa. The reason can be attributed to excessive chemical reaction taking place at interface when holding time is further increased. The reaction causes large quantity of intermetallic ternary carbides

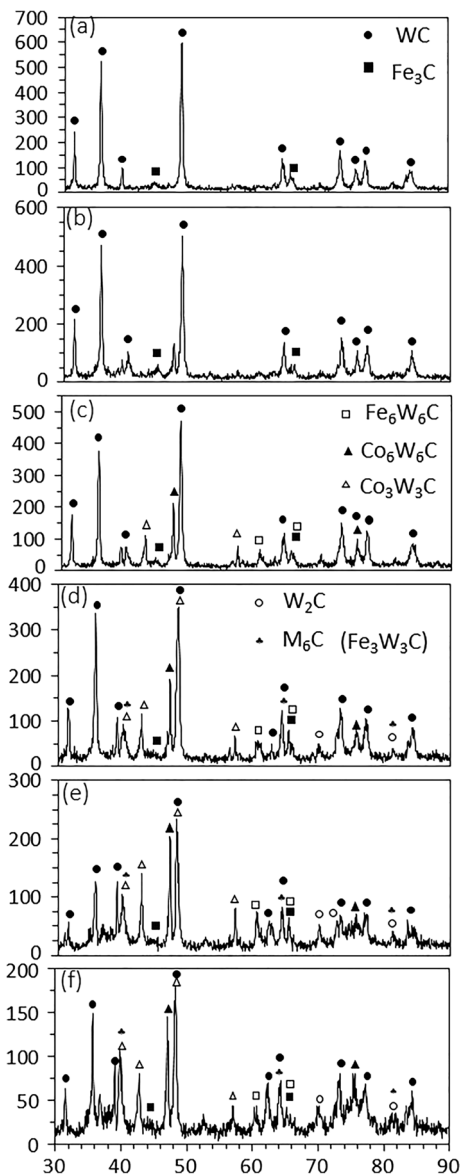


Fig. 8 X-ray diffraction patterns of WC-10Co/AISI 4340 composite materials showing the effects of holding times at (a) 5 min, (b) 10 min, (c) 20 min, (d) 30 min, (e) 40 min and (f) 50 min, sintered at 1200°C under compaction pressure of 160 MPa

Table 2 Phase information of the bilayered composite from MAUD software

Phase	Crystal system	Space group	Cell parameters (Å)
WC	Hexagonal	P6m2	$a = 2.90, c = 2.84$
Fe ₃ C	Orthorhombic	Pnma	$a = 5.27, b = 6.58, c = 4.36$
W ₂ C	Trigonal	P31 m	$a = 5.19, c = 4.724$
Fe ₆ W ₆ C	Cubic	Fd3 m	$a = 10.93$
Co ₆ W ₆ C	Cubic	Fd3 m	$a = 20.61$
Fe ₃ W ₃ C	Cubic	Fd3 m	$a = 7.97$
Co ₃ W ₃ C	Cubic	Fd3 m	$a = 7.79$

to form as identified by XRD results. Since these carbides are brittle in nature, their presence in large quantity results in the decrement of the bonding strength. This justification is also in line with the microstructure analysis as shown in Fig. 6(e), that the diffusion layer becomes thicker at holding time of 50 min.

3.3.2 Microhardness. To evaluate the mechanical properties of the sintered cemented tungsten carbide, indentation microhardness profile is obtained by Vickers microhardness tester with a distance of about 150 μm between two successive indentations. The obtained results are presented in Fig. 10. Figure 2(a) shows the schematic diagram of the indentation measurement points, in which, 12 points from cermet region (6 from each side) and 5 points from steel region are taken into account. The standard deviation was calculated by considering 3-4 sets of line data for every sample. In cemented tungsten carbide, WC is embedded into Co matrix, owing to possess high hardness, which in turn, makes it one of the widely used wear-resistant materials, as it is well known that higher hardness demonstrates increased wear performance (Ref 22, 52). A trend of increasing hardness due to increase in holding time is observed. At lower holding times such as 5 and 10 min, the hardness values are as low as 200-500 HV, because of incomplete densification and presence of large volume porosity. The microhardness, however, in steel section is found similar, with only a slight change due to change in sintering time. Comparing to conventional hardness of martensite (300 to 700 HV) at 0.4% C, a slight increase of hardness (500 to 800 HV) is observed, which is probably because of slight migration of C from carbide region to steel region (Ref 53) due to concentration difference, though penetration of C elements is not clearly identified by EDS scanning analysis. Further increase in sintering time causes continuous improvement of the hardness. The average maximum hardness achieved is 1984 HV [99.5% relative to conventional hardness of nanocrystalline WC-10Co (Ref 54)] with sintering time of 50 min, while the average is 1845.71 HV. This demonstrates the possibility of achieving high density of carbide materials at comparatively lower temperature by means of hot compaction diffusion sintering process. Another reason of achieving such high hardness is attributed to the use of nanocrystalline powder (Ref 21). The mechanical properties, e.g., hardness, of cemented tungsten carbide using nano-sized WC-Co powders are significantly higher than what could be achieved using conventional powders. The use of HCDB mechanism led to the formation of hard complex carbide mesophases like Co₆W₆C, Co₃W₃C, Fe₆W₆C and WC, as identified by the XRD spectrum, and caused to increase microhardness of the sintered carbides (Ref 22).

3.3.3 Density and Porosity Analysis. Owing to the facilities of heating and pressurizing simultaneously, hot compaction diffusion process offers the advantage of achieving high densification at lower temperature by rapid elimination of porosity and voids (Ref 1). Figure 11 shows the results of density and porosity measurements of nanocrystalline WC-10Co powder; the corresponding SEM image is referred to Fig. 6. As shown in Fig. 6(a), the microstructure prepared at holding time of 5 min has high volume of porosity and voids, leading to an average density as low as 8.67 g/cm³ [59.72% theoretical density (TD)]. The density was obtained by

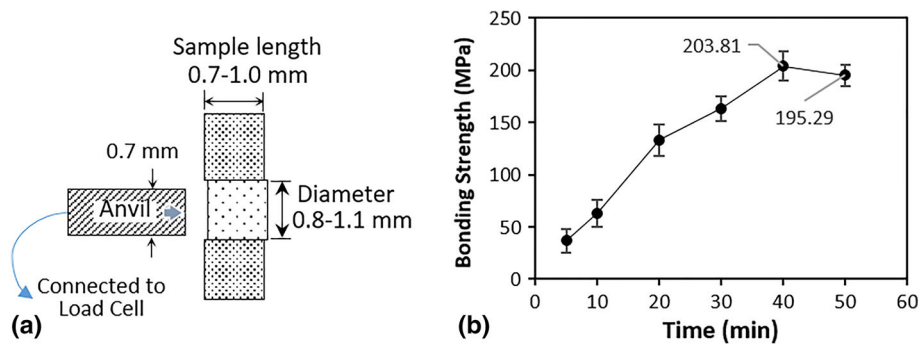


Fig. 9 Determination of bonding shear strength with the variation of holding time, (a) the schematic diagram showing the bonding shear strength test mechanism using high-precision micro-tensile test machine and (b) bonding shear strength results obtained at different holding times from 5 to 50 min

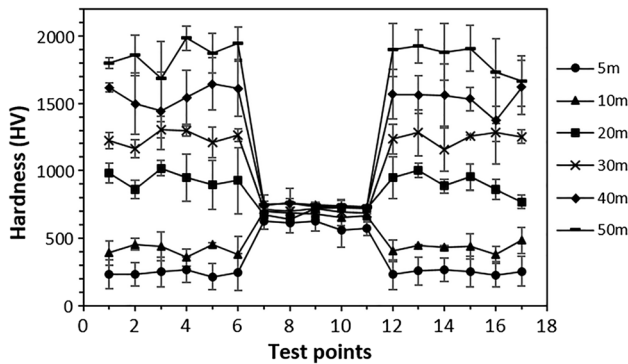


Fig. 10 Microhardness profiles of the WC-10Co/AISI 4340 steel bilayered composite presented as a function of distance showing the effects of holding time during sintering process

measuring the weight of the powders used before the experiment and then calculating the final volume occupied by the sintered powders. Since the final product is cylindrical shaped with an insert of steel in the middle, the volume of WC-10Co was measured by calculating the total volume of the composite and then deducting the volume of the steel insert. Digital Vernier calliper was used to measure the dimensions to ensure the accuracy. As can be seen, the density continues to increase

with the increase in sintering time (Fig. 11a). In stage (1), at holding time ≤ 20 min, the rate of densification growth is higher. In stages (2) and (3), the density continues to increase, however, at a slower rate. It can be noted that the inter-particle gaps decrease with the increase in sintering time, resulting in increase in density. Such analysis was also conducted by Sun et al. (Ref 29). This is because, at elevated temperature and pressure, inter-particle gaps or pores start to reduce, the more the time allowed more the elimination of pores and higher the density. The average maximum density achieved is 95.92% TD at 50 min of sintering time. Further increase in density could be possible to reach by increasing initial green density which, in this experiment, was limited to 12-15% TD. Since the green density was obtained by pressing of WC-10Co powder inside the quartz tube manually, there was a possibility of breaking the quartz tube if high pressure applied. The loose green density causes to upsurge the presence of voids among powder particles which hinders the solidification process. Moreover, comparing to previous studies (Ref 21), we achieved higher density of cemented tungsten carbide at 1200°C, using HCDB process.

The presence of porosity decreases the mechanical performance of the materials particularly in the application where abrasion, wear, surface fatigue, spalling and dislodgement are involved (Ref 22). Studies show that the amount of porosity in hard metals has marked effect on their properties. For example, the residual porosity in WC-10Co alloys can decrease their transverse rupture strength from 340 to 290 kg/mm² as reported

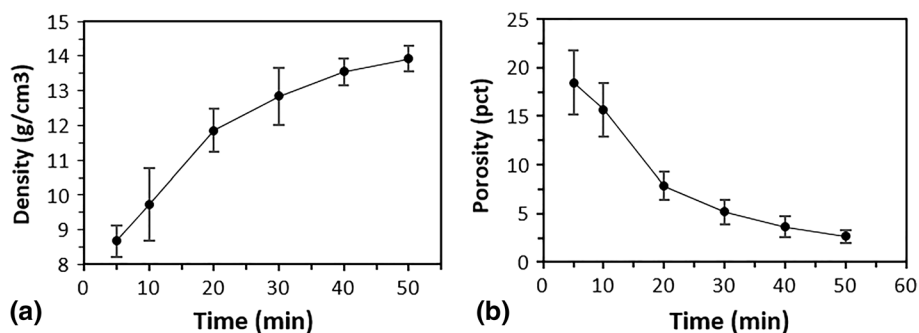


Fig. 11 Analysis of density and porosity of the sintered cermet: (a) density obtained at different holding times, and (b) porosity assessment at different holding times, sintered at 1200°C, under constant compression pressure of 160 MPa

in Ref 55. Thus, it underlines the significance of evaluating the porosity of the cemented tungsten carbide. The porosity assessment was conducted by using a commercially available image analysis software tool (ImageJ 1.48v, USA) on the images acquired by SEM. The obtained results are presented in Fig. 11(b) with their relative standard deviations, where each of the data is an average of 3-6 samples. The porosity observed has a decrement tendency with the increase in holding time. The maximum porosity reported to be 18.45% at 5 min of sintering time, indicating that the carbides are encountered with poor density, which is also reflected in the results of density analysis. With the increase in holding time, the porosity continues to reduce; however, a sharp drop of porosity is observed when the sintering time is raised from 10 to 20 min. After this, the porosity decreases slowly to a minimum value of 2.63% as shown in Fig. 11(b).

4. Conclusions

The effects of holding time on microstructure and mechanical properties of WC-10Co/AISI 4340 dissimilar bilayered composite produced by powder–solid hot compaction diffusion bonding at low temperature were examined, and following conclusions are made.

- a. A powder–solid diffusion bonding process was successfully used to fabricate a bilayered composite of WC-10Co and AISI 4340 steel at a temperature of 1200°C. The holding time (5-50 min) greatly influences the interfacial microstructure and mechanical properties of the bonds.
- b. Good metallurgical bonding and defects free contacts at the interface were inferred from microstructural analysis. When holding time reaches over 20 min, intermetallic ternary carbides start to form at the bonding interface and continue to grow with the increase in holding time.
- c. The depth of transitional layer generated due to interdiffusion of alloying elements increased with the increase in time. The intermetallic compounds formed at the interface are identified and found to be well matched according to the prediction conducted by thermodynamic simulation.
- d. Based on holding time examined, the results can be classified as: stage (1) holding time ≤ 20 min; the WC-10Co powders were poorly sintered and mechanical properties including bonding strength are limited. Stage (2) $20 < \text{holding time} \leq 40$ min, the mechanical properties of the sintered carbide improved considerably and the maximum bonding strength achieved at holding time of 40 min. And stage (3) holding time > 40 min, the mechanical properties (density and microhardness) improved, but bonding strength reduced. The presence of high volume brittle intermetallic phases reduced the bonding strength. Based on those, 40 min holding is considered to be optimal holding time.
- e. Compared to other techniques, hot compaction diffusion bonding process can reduce the requirement of sintering ceramic materials at high temperature and obtain a strong and stable bonding with steel.

Acknowledgments

The authors would like to thank the Australian Research Council (ARC) for its financial support for the current study. We also acknowledge the use of facilities within the UOW Electron Microscopy Centre.

References

1. M. Hasan et al., Analysis of Sintering and Bonding of Ultrafine WC Powder and Stainless Steel by Hot Compaction Diffusion Bonding, *Fusion Eng. Des.*, 2018, **133**, p 39–50
2. A. Thomazic, C. Pascal, and J.M. Chaix, Fabrication of (Cemented Carbides/Steel) Bilayered Materials by Powder Metallurgy, *Materials Science Forum*, Vols. 631–632, Trans Tech Publications Ltd., 2010, p 239–244
3. M. Hasan, J. Zhao, and Z. Jiang, A Review of Modern Advancements in Micro Drilling Techniques, *J. Manuf. Process.*, 2017, **29**, p 343–375
4. C. Pascal et al., Pressureless Co-sintering Behaviour of a Steel/Cemented Carbide Component: model Bimaterial, *Int. J. Mater. Res.*, 2012, **103**(3), p 296–308
5. Y. Zheng et al., Preparation and Mechanical Properties of TiC-Fe Cermets and TiC-Fe/Fe Bilayer Composites, *J. Mater. Eng. Perform.*, 2017, **26**(10), p 4933–4939
6. A.K. Maiti, N. Mukhopadhyay, and R. Raman, Improving the Wear Behavior of WC-CoCr-Based HVOF Coating by Surface Grinding, *J. Mater. Eng. Perform.*, 2009, **18**(8), p 1060
7. K. Feng et al., Investigation on Diffusion Bonding of Functionally Graded WC-Co/Ni Composite and Stainless Steel, *Mater. Des.*, 2013, **46**, p 622–626
8. W.-B. Lee, B.-D. Kwon, and S.-B. Jung, Effects of Cr_3C_2 on the Microstructure and Mechanical Properties of the Brazed Joints Between WC-Co and Carbon Steel, *Int. J. Refract. Met. Hard Mater.*, 2006, **24**(3), p 215–221
9. J. Bao, J.W. Newkirk, and S. Bao, Wear-Resistant WC Composite Hard Coatings by Brazing, *J. Mater. Eng. Perform.*, 2004, **13**(4), p 385–388
10. X.Z. Zhang et al., Vacuum Brazing of WC-8Co Cemented Carbides to Carbon Steel Using Pure Cu and Ag-28Cu as Filler Metal, *J. Mater. Eng. Perform.*, 2017, **26**(2), p 488–494
11. S. Giménez et al., Chemical Reactivity of PVD-Coated WC-Co Tools with Steel, *Appl. Surf. Sci.*, 2007, **253**(7), p 3547–3556
12. Z. Zhong et al., Microstructure and Mechanical Properties of Diffusion Bonded Joints Between Tungsten and F82H Steel Using a Titanium Interlayer, *J. Alloy. Compd.*, 2010, **489**(2), p 545–551
13. M. Barrena, J.G. De Salazar, and L. Matesanz, Interfacial Microstructure and Mechanical Strength of WC-Co/90MnCrV8 Cold Work Tool Steel Diffusion Bonded Joint with Cu/Ni Electroplated Interlayer, *Mater. Des.*, 2010, **31**(7), p 3389–3394
14. J. Missiaen et al., Design of a W/Steel Functionally Graded Material for Plasma Facing Components of DEMO, *J. Nucl. Mater.*, 2011, **416**(3), p 262–269
15. Z.-H. Yang et al., Tungsten/Steel Diffusion Bonding Using Cu/W-Ni/Ni Multi-interlayer, *Trans. Nonferrous Met. Soc. China*, 2014, **24**(8), p 2554–2558
16. T. Grunder et al., Residual Stress in Brazing of Submicron Al_2O_3 to WC-Co, *J. Mater. Eng. Perform.*, 2016, **25**(7), p 2914–2921
17. T. Hirose et al., Joining Technologies of Reduced Activation Ferritic/Martensitic Steel for Blanket Fabrication, *Fusion Eng. Des.*, 2006, **81**(1), p 645–651
18. H. Greuner et al., Vacuum Plasma-Sprayed Tungsten on EUROFER and 316L: Results of Characterisation and Thermal Loading Tests, *Fusion Eng. Des.*, 2005, **75**, p 333–338
19. M. Rosinski et al., W/Cu Composites Produced by Pulse Plasma Sintering Technique (PPS), *Fusion Eng. Des.*, 2007, **82**(15), p 2621–2626
20. C. Pascal, et al. Elaboration of (steel/cemented carbide) multimaterial by powder metallurgy, in *Materials Science Forum* (Trans Tech Publ, 2007)
21. Z.Z. Fang et al., Synthesis, Sintering, Mechanical Properties of Nanocrystalline Cemented Tungsten Carbide—A Review, *Int. J. Refract. Met. Hard Mater.*, 2009, **27**(2), p 288–299

22. S. Zafar and A.K. Sharma, Development and Characterisations of WC-12Co Microwave Clad, *Mater. Charact.*, 2014, **96**, p 241–248
23. C. Pascal et al., Design of Multimaterial Processed by Powder Metallurgy: Processing of a (Steel/Cemented Carbides) Bilayer Material, *J. Mater. Process. Technol.*, 2009, **209**(3), p 1254–1261
24. S. Takemoto et al., Diffusion of Tungsten in α -Iron, *Philos. Mag.*, 2007, **87**(11), p 1619–1629
25. Y. Shinoda, T. Akatsu, and F. Wakai, Integrated Molding of Nanocrystalline Tungsten Carbide Powder with Stainless Steel, *Mater. Sci. Eng., B*, 2008, **148**(1), p 145–148
26. C.P. Paul et al., Cladding of WC-12 Co on Low Carbon Steel Using a Pulsed Nd:YAG Laser, *Mater. Sci. Eng., A*, 2007, **464**(1), p 170–176
27. G. Goren-Muginstein, S. Berger, and A. Rosen, Sintering Study of Nanocrystalline Tungsten Carbide Powders, *Nanostruct. Mater.*, 1998, **10**(5), p 795–804
28. J.S. Xu et al., Microstructure and Sliding Wear Resistance of Laser Cladded WC/Ni Composite Coatings with Different Contents of WC Particle, *J. Mater. Eng. Perform.*, 2012, **21**(9), p 1904–1911
29. L. Sun, C.-C. Jia, and M. Xian, A research on the Grain Growth of WC-Co Cemented Carbide, *Int. J. Refract. Met. Hard Mater.*, 2007, **25**(2), p 121–124
30. P. Arato et al., Solid or Liquid Phase Sintering of Nanocrystalline WC/Co Hardmetals, *Nanostruct. Mater.*, 1998, **10**(2), p 245–255
31. H. Lukas, S.G. Fries, and B. Sundman, *Computational Thermodynamics: The Calphad Method*, Cambridge University Press, Cambridge, 2007
32. S. Haglund and J. Ågren, W Content in Co Binder During Sintering of WC-Co, *Acta Mater.*, 1998, **46**(8), p 2801–2807
33. A. Petersson, *Cemented Carbide Sintering: Constitutive Relations and Microstructural Evolution*, Department of Materials Science and Engineering, Royal Institute of Technology, Högskoletyckeriet, Stockholm, 2004
34. The Welding Institute, *What are The Microstructural Constituents Austenite, Martensite, Bainite, Pearlite and Ferrite?*, 2018. <https://www.twi-global.com/technical-knowledge/faqs/faq-what-are-the-microstructural-constituents-austenite-martensite-bainite-pearlite-and-ferrite/>. Accessed 15 Jan 2018
35. A.S.F. Metals, *Atlas of Isothermal Transformation and Cooling Transformation Diagrams*, American Society for Metals, Russell Township, 1977
36. W.W. Basuki and J. Aktaa, Diffusion Bonding Between W and EUROFER97 Using V Interlayer, *J. Nucl. Mater.*, 2012, **429**(1), p 335–340
37. W. Basuki and J. Aktaa, Investigation of Tungsten/EUROFER97 Diffusion Bonding Using Nb Interlayer, *Fusion Eng. Des.*, 2011, **86**(9), p 2585–2588
38. Z. Zhong, T. Hinoki, and A. Kohyama, Effect of Holding Time on the Microstructure and Strength of Tungsten/Ferritic Steel Joints Diffusion Bonded with a Nickel Interlayer, *Mater. Sci. Eng., A*, 2009, **518**(1), p 167–173
39. T.T. Sasaki et al., Microstructural Evolution of copper Clad Steel Bilayered Wire, *Mater. Sci. Eng., A*, 2011, **528**(6), p 2974–2981
40. L. Dong et al., Metallurgical Process Analysis and Microstructure Characterization of the Bonding Interface of QA19-4 Aluminum Bronze and 304 Stainless Steel Composite Materials, *J. Mater. Process. Technol.*, 2016, **238**, p 325–332
41. D.V. Suetin, I.R. Shein, and A.L. Ivanovskii, Structural, Electronic and Magnetic Properties of η Carbides (Fe₃W₃C, Fe₆W₆C, Co₃W₃C and Co₆W₆C) from first Principles Calculations, *Phys. B*, 2009, **404**(20), p 3544–3549
42. I.F. Machado et al., The Study of Ternary Carbides Formation During SPS Consolidation Process in the WC-Co-Steel System, *Int. J. Refract Metal Hard Mater.*, 2009, **27**(5), p 883–891
43. N.A. Dubrovinskaia et al., Thermal Expansion and Compressibility of Co₆W₆C, *J. Alloy. Compd.*, 1999, **285**(1), p 242–245
44. A.R. Trueman, D.P. Schweinsberg, and G.A. Hope, A Study of the Effect of Cobalt Additions on the Corrosion of Tungsten Carbide/Carbon Steel Metal Matrix Composites, *Corros. Sci.*, 1999, **41**(7), p 1377–1389
45. H. Li et al., Microstructure Modifications and Phase Transformation in Plasma-Sprayed WC-Co Coatings Following Post-Spray Spark Plasma Sintering, *Surf. Coat. Technol.*, 2005, **194**(1), p 96–102
46. D. Gupta and A.K. Sharma, Microstructural Characterization of Cermets Cladding Developed Through Microwave Irradiation, *J. Mater. Eng. Perform.*, 2012, **21**(10), p 2165–2172
47. V. Ramnath and N. Jayaraman, Quantitative Phase Analysis by X-Ray Diffraction in the Co-W-C System, *J. Mater. Sci. Lett.*, 1987, **6**(12), p 1414–1418
48. Q.-B. Yang and S. Andersson, Application of Coincidence Site Lattices for Crystal Structure Description. Part I: $\Sigma = 3$, *Acta Crystallogr. Sect. B*, 1987, **43**(1), p 1–14
49. P.Q. Xu et al., Analysis of Formation and Interfacial WC Dissolution Behavior of WC-Co/Invar Laser-TIG Welded Joints, *J. Mater. Eng. Perform.*, 2013, **22**(2), p 613–623
50. A. Bansal, S. Zafar, and A.K. Sharma, Microstructure and Abrasive Wear Performance of Ni-Wc Composite Microwave Clad, *J. Mater. Eng. Perform.*, 2015, **24**(10), p 3708–3716
51. X. Gao et al., Effects of Temperature and Strain Rate on Microstructure and Mechanical Properties of High Chromium Cast Iron/Low Carbon Steel Bilayered Prepared by Hot Diffusion-Compression Bonding, *Mater. Des.*, 2014, **63**, p 650–657
52. L. Zhong et al., Microstructural and Mechanical Properties of In Situ WC-Fe/Fe Composites, *J. Mater. Eng. Perform.*, 2015, **24**(11), p 4561–4568
53. G. Krauss, Martensite in Steel: Strength and Structure, *Mater. Sci. Eng., A*, 1999, **273–275**, p 40–57
54. C. Steinbach, *Tungsten Carbide-Cobalt—Material Information*, Information About Nanomaterials and Their Safety Assessment, 2014. <https://www.nanopartikel.info/en/nanoinfo/materials/tungsten-carbide-cobalt/material-information#literatur>. Accessed 5 Mar 2017
55. N. Romanova, G. Kreimer, and V. Tumanov, Effects of Residual Porosity on the Properties of Tungsten Carbide-Cobalt Hard Alloys, *Sov. Powder Metall. Met. Ceram.*, 1974, **13**(8), p 670–673

Publisher's Note Springer Nature remains neutral with regard to jurisdictional claims in published maps and institutional affiliations.